ACS APPLIED MATERIALS & INTERFACES

Research Article

www.acsami.org

High-Energy Dissipation Performance in Epoxy Coatings by the Synergistic Effect of Carbon Nanotube/Block Copolymer Conjugates

Hernan Garate,*[,†,⊥,¶] Micaela Bianchi,[§] Lía I. Pietrasanta,[§,‡] Silvia Goyanes,[⊥,‡] and Norma B. D'Accorso*[,†]

[†]CIHIDECAR-CONICET, Departamento de Química Orgánica, FCEyN-UBA, [§]Centro de Microscopías Avanzadas, FCEyN-UBA, [⊥]LP&MC, and [‡]IFIBA-CONICET, Departamento de Física, FCEyN-UBA, Ciudad Universitaria, 1428, Ciudad Autónoma de Buenos Aires, Argentina

Supporting Information

ABSTRACT: Hierarchical assembly of hard/soft nanoparticles holds great potential as reinforcements for polymer nanocomposites with tailored properties. Here, we present a facile strategy to integrate polystyrene-grafted carbon nanotubes (PSgCNT) (0.05−0.3 wt %) and poly(styrene-*b*-[isoprene-*ran*-epoxyisoprene]-*b*-styrene) block copolymer (10 wt %) into epoxy coatings using an ultrasound-assisted noncovalent functionalization process. The method leads to cured nanocomposites with core−shell block copolymer (BCP) nanodomains which are associated with carbon nanotubes (CNT) giving rise to CNT−BCP hybrid structures. Nanocomposite energy dissipation and reduced Young's Modulus (E^*) is determined from force−distance curves by atomic force microscopy operating in the PeakForce QNM imaging mode and compared to thermosets modified with BCP and purified carbon nanotubes (pCNT). Remarkably, nanocomposites bearing PSgCNT−BCP conjugates display an increase in energy dissipation of up to 7.1-fold with respect to neat epoxy and 53% more than materials prepared with pCNT and BCP at the same CNT load (0.3 wt %), while reduced Young's Modulus shows no significant change with CNT type and increases up to 25% compared to neat epoxy E^* at a CNT load of 0.3 wt %. The energy dissipation performance of nanocomposites is also reflected by the lower wear coefficients of materials with PSgCNT and BCP compared to those with pCNT and BCP, as determined by abrasion tests. Furthermore, scanning electron microscopy (SEM) images taken on wear surfaces show that materials incorporating PSgCNT and BCP exhibit much more surface deformation under shear forces in agreement with their higher ability to dissipate more energy before particle release. We propose that the synergistic effect observed in energy dissipation arises from hierarchical assembly of PSgCNT and BCP within the epoxy matrix and provides clues that the CNT−BCP interface has a significant role in the mechanisms of energy dissipation of epoxy coating modified by CNT−BCP conjugates. These findings provide a means to design epoxy-based coatings with high-energy dissipation performance.

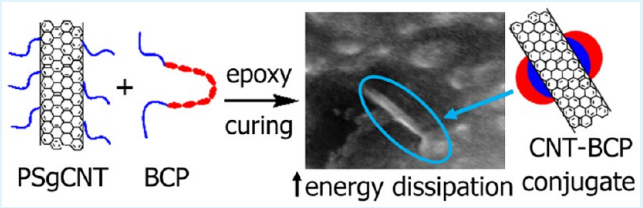

KEYWORDS: *epoxy coatings, block copolymer (BCP), carbon nanotubes (CNT), energy dissipation, wear resistance, nanocomposites*

INTRODUCTION

Engineered multifunctional polymer nanocomposites have attracted great attention in the past few years due to the increasing demand of mechanically stable and durable materials for advanced high-performance applications.[1−3] Nanocomposites incorporating hierarchically structured nano-objects offer attractive opportunities to generate tailored materials with useful properties not accessible with traditional nanocomposites.[4,5]

However, introduction of multiple nanoelements to a polymer matrix often leads to phase separation, incompatibility, and inhomogeneity issues. Therefore, the development of complex multicomponent materials requires a rational design oriented to stabilize the interfaces between its constituents.[3] Among nanofillers, carbon nanotubes (CNT) have been subjected to intensive research because they combine large aspect ratio, low density (~1.3 g·mL^{-1}), and high surface area per mass and volume with outstanding mechanical, electrical, and thermal properties, which should make them an ideal filler to impart these multifunctionalities to the host polymeric matrices.[6,7] However, the tendency of CNT to aggregate due to strong van der Waals interactions has limited their potential. In order to circumvent the latter drawback, several studies have demonstrated that surface functionalization of CNT significantly enhances polymer nanocomposite properties by reducing CNT agglomeration and increasing effective matrix−filler load transfer.[8−13] In this regard, block copolymers (BCP) have been extensively used to assist CNT dispersions within polymer/CNT composites.[14−16] Apart from being used as CNT dispersing agents, BCP have also been widely investigated as polymer modifiers due to their ability to self-assemble into various well-defined morphologies at the nanometer scale that

Received: October 17, 2016
Accepted: December 6, 2016
Published: December 6, 2016

DOI: 10.1021/acsami.6b13212
ACS Appl. Mater. Interfaces 2017, 9, 930−943

serve to enhance several material properties such as surface properties and toughness.[17−20]

Recent articles demonstrated that a combination of CNT and BCP results in a hybrid nanoscale architecture that simultaneously integrates properties of its constituents.[15,21−24] The design of CNT−BCP conjugates was oriented to form a close interaction between one block of the BCP and the carbon nanotube walls (for instance by $\pi-\pi$ interaction),[21,23] while a second block phase separates into a second phase due to the incompatibility with the former block. For instance, Jia et al. described a method to prepare CNT−BCP hybrid structures by crystallization-driven self-assembly of polyferrocenyldimethylsilane-*b*-polyisoprene block copolymer and CNT.[21] Yang et al. obtained hierarchical core−shell hybrids by noncovalent functionalization of CNT with poly(ethylene oxide)-*b*-polyaniline, where the polyaniline subchains absorbed on the CNT surface by $\pi-\pi$ interaction.[23] More recently, the formation of CNT−BCP patchy conjugates by noncovalent functionalization of CNT with polystyrene-*b*-polyethylene-*b*-poly(methyl methacrylate) triblock copolymer was described,[15] and their potential use as reinforcements in polymer blend nanocomposites was suggested.[24] However, articles investigating material properties of epoxy thermosets modified with CNT and BCP are scarce,[25−27] and significant improvements on material properties are yet to be achieved. For instance, Martin-Gallego et al.[27] reported an increment of ∼15% in the critical stress intensity factor with respect to neat epoxy for an epoxy nanocomposite bearing multiwalled carbon nanotubes (0.25 wt %) and poly(ethylene oxide)−poly(propylene oxide)−poly(ethylene oxide) BCP (10 wt %), while the addition of CNT (0.25 wt %) or BCP (10 wt %) led to increments of ∼13% with the same property compared to neat epoxy. Furthermore, to the best of our knowledge the impact of CNT−BCP conjugates on polymer nanocomposite mechanical properties has not been previously addressed.

Therefore, in this Article, we show the effect of incorporating CNT and BCP, which are capable of coassembling into CNT−BCP conjugates, on relevant physical properties of thin epoxy coatings with applications in the aerospace industry. From the technological point of view, we are interested in finding a practically feasible way of increasing energy dissipation and electrical conductivity of the epoxy system without the detriment of other epoxy properties such as Young's Modulus and wear resistance, which are of vital importance in the lifecycle of epoxy coatings.

Our approach toward multicomponent epoxy nanocomposites consists of integrating self-assembled poly(styrene-*b*-[isoprene-*ran*-epoxyisoprene]-*b*-styrene) (eSIS) block copolymer and polystyrene-grafted carbon nanotubes. In such multicomponent material, CNT would contribute to energy dissipation[28] and provide electrical conductivity, while BCP nanodomains would assist CNT dispersion by noncovalent functionalization and act as energy-dissipative elements.[29] eSIS was selected on the basis that PS subchains can interact with CNT walls by $\pi-\pi$ stacking,[30,31] while epoxidized polyisoprene subchains are compatible with the epoxy precursors before curing.[32] Nanocomposite energy dissipation was systematically investigated by atomic force microscopy using the PeakForce QNM imaging mode, and material wear resistance was obtained by abrasion tests and compared to nanocomposites bearing purified CNT and BCP. Our results show that formation of polystyrene-grafted carbon nanotubes (PSgCNT)−BCP hybrid structures within the epoxy matrix exerts a synergistic effect in energy dissipation, providing a means for designing epoxy coatings with optimal mechanical properties.

EXPERIMENTAL SECTION

Materials. A commercial cylinder forming poly(styrene-*b*-isoprene-*b*-styrene) (SIS) block copolymer Kraton SIS-D1165 (PS content 30 wt %) with a M_w of 145 000 g/mol and a PDI = 1.5, as determined by gel permeation chromatography, was epoxidized in 85% (eSIS) using dimethyldioxirane as the epoxidizing agent following a previously reported strategy.[33] The product was characterized by size exclusion chromatography: M_w of eSIS, 165 000 g/mol; M_w of PS blocks ∼22 000 g/mol; PDI = 1.7. (Gel permeation chromatography traces for SIS and eSIS are provided in the Supporting Information.) Multiwalled carbon nanotubes (Nanocyl NC3100) were purified by a method described in a previous reference.[30] Purified CNT (pCNT) had an outer and inner diameter of 15 and 7 nm, respectively, and an average length of 3 μm. Multiwalled carbon nanotubes grafted with PS chains (PSgCNT) having a lower mean molecular weight than the PS blocks of eSIS were prepared and characterized in a previous work.[30] PSgCNT contain 89 wt % of CNT and 11 wt % of PS. The PS chains grafted to the CNT have a M_w ∼ 12 000 g/mol and a polydispersity index of 1.3. The grafting density was calculated to be 5.2×10^3 PS chains per nanotube.[30] No significant differences in CNT aspect ratio were found between pCNT and PSgCNT.[30] The epoxy monomer, diglycidyl ether of bisphenol A (DGEBA), Epikote 828, was purchased from Hexion. It has an epoxy equivalent of ∼184−190. The hardener was a mixture of amines under the commercial name of Ancamine 2500 (1-(2-aminoethyl)-piperazine (AEP)/1,3-bis(aminomethyl)-benzene (*m*-XDA); 1:2 mol/mol), supplied by Air Products. The chemical formula of all the epoxy components and CNT used in this work are given in Figure 1.

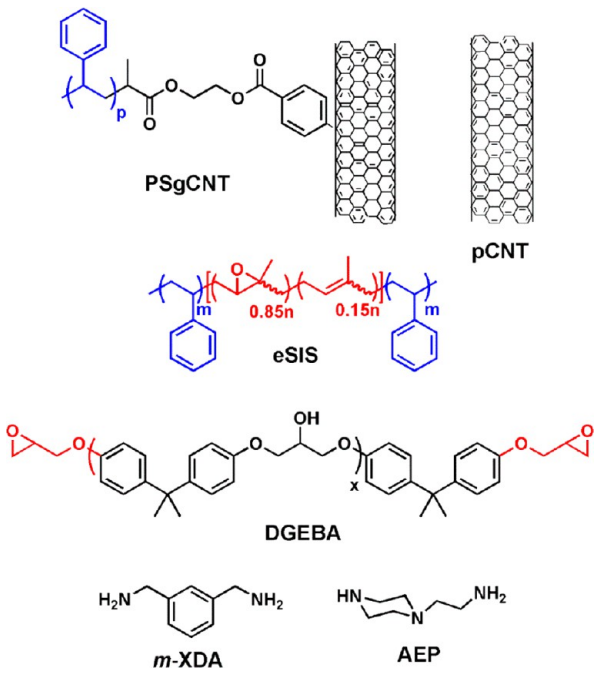

Figure 1. Epoxy components and block copolymers used in this study.

Nanocomposite Preparation. DGEBA/hardener and all epoxy nanocomposite blends were prepared to provide a stoichiometric balance between amine protons and epoxy groups. Film nanocomposites with a block copolymer content of 10 wt % and pCNT or PSgCNT in the range of 0.05−0.3 wt % were prepared as follows: PSgCNT or pCNT (at the same weight fraction) were dispersed in toluene (Merck) (135 mL) under ultrasonic vibration (80 W) for 15 min. Dodecanethiol (DT) (Sigma-Aldrich) (5.5 mL) was added as a

DOI: 10.1021/acsami.6b13212
ACS Appl. Mater. Interfaces 2017, 9, 930−943

cosolvent in order to aid PSgCNT dispersion.[30] The resulting CNT dispersions were further sonicated for 15 min; eSIS (1.0191 g, 7.9 mmol of epoxy) was then added to the obtained dispersion and sonicated for 60 min. DGEBA (5.8588 g, 31.1 mmol of epoxy) was dissolved and sonicated for a further 30 min. Ancamine (3.3027 g, 39.0 mmol of −NH) was then added to the resulting dispersion. After a last step of ultrasonic vibration for 5 min, the dispersions were drop-casted on silicon substrates (~30 μL/4 cm^2), previously cleaned with acetone and ethanol, and dried with high purity nitrogen. The solvent was evaporated at 25 °C for 24 h (1 atm). It is worth noting that DT does not react to DGEBA at room temperature due to the absence of a strong base capable of abstracting the proton − *SH* from DT[34] (pK_a values for DT = 11; AEP = 9.5; *m*-XDA = 9). The final stage of drying was at 25 °C for 2 h under vacuum (~1.10^{-3} Torr) to evaporate DT[35] (vapor pressure of 2.5 Torr at 25 °C). Epoxy resin was subsequently cured at 80 °C for 180 min under vacuum (~1.10^{-3} Torr). The obtained films had a thickness in the range of 1.5−6 μm, as determined by a digital micrometer. Epoxy nanocomposites were identified as epoxy/eSIS/pCNT_*x* and epoxy/eSIS/PSgCNT_*x* for samples containing pCNT and PSgCNT, respectively, where *x* refers to the CNT content (wt %). The curing process was considered to be completed after curing for 3 h at 80 °C since the epoxy glass transition temperature showed no significant change between the first and second heating scans in differential scanning calorimetry (DSC) experiments. Moreover, no residual reaction exotherm was detected in the first DSC heating scan (between 25 and 150 °C at a rate of 20 °C/min) in agreement with a complete curing process. The absence of residual solvent was also confirmed by DSC as no significant change was observed in T_g values between cured DGEBA/hardener films prepared with toluene as solvent and with a toluene/DT mixture.

The curing process was further characterized by isothermal DSC experiments at 80 °C for 3 h. ΔH values of ~100 kJ/mol were estimated from the reaction exotherm, consistent with that for epoxy-amine polycondensation[36] and well below reported ΔH values for thiol-epoxy reaction (~130 kJ/mol)[37,38] On the other hand, at the curing temperature, DGEBA homopolymerization initiated by AEP is unlikely to occur as this reaction takes place at ~122 °C (Supporting Information).

Thermal Analysis. Differential scanning calorimetry measurements were made on a TA Q20 differential scanning calorimeter under a dry nitrogen atmosphere. Indium standard was used for calibration. Dynamic experiments were performed to obtain the T_g values of nanostructured thermosets. Films were first removed from the substrate and placed (5−10 mg) in the DSC pan. Samples were heated to 150 °C, and the temperature was held for 10 min to remove the thermal history. Subsequently, samples were cooled to −80 °C for 15 min and heated to 150 °C at a rate of 20 °C/min. All T_g values were taken as the midpoint of the transition in the second heating scan.

Electrical Conductivity. Electrical conductivity σ was determined from resistivity measurements carried out by standard four-point measurement using a Keithley 199 Systems DMM/Scanner digital multimeter. Nanocomposite films were deposited over Al substrates. After measuring film thickness with a digital micrometer, a thin platinum layer was sputtered in the top surface of each film, and then, the edges were cut using a metallic punch (17 mm diameter) to ensure a constant area and avoid edge effects in the electrical measurement. Electrical conductivity in the thickness direction was calculated from eq 1:

$$\sigma = \frac{e}{Ra} \tag{1}$$

where e is the nanocomposite film thickness, R is the electrical resistance, and a is the film surface area. The electrical conductivity measurement was repeated 5 times on 3 different specimens for each sample to ensure accuracy.

Atomic Force Microscopy (AFM). AFM experiments, imaging of surface topography (AFM tapping mode and Phase) and surface material properties (PeakForce QNM), were performed with a Bruker Multimode 8 AFM with a Nanoscope V controller (Santa Barbara, CA, USA) and the software NanoScope 8.15. PeakForce QNM[39] is a recently introduced atomic force microscopy imaging mode based on the acquisition of force curves recorded at each pixel of the topographic image. The force curves are analyzed instantaneously, and the quantification of the nanomechanical properties such as adhesion, Young's Modulus, dissipation, and deformation is possible. The studies were carried out in a dry nitrogen atmosphere using silicon rectangular cantilevers with rotated pyramidal tips. The Etched Silicon Probe with Rotated Tip (RTESP) probe (Bruker) specifications include a nominal tip radius of 8 nm curvature, nominal cantilever spring constant k of 40 N/m, and nominal resonant frequency of 300 kHz. Before each measurement, the spring constant was calibrated in air using the thermal noise method.[40] The AFM tip radius was measured using the standard polycrystalline titanium roughness sample provided by Bruker and the Tip Qualification function in NanoScope Analysis software. The deflection sensitivity was determined using a hard sample, such as the sapphire sample provided by Bruker. The deflection and *z*-position data were recorded at a sampling rate of 2 kHz and peak force amplitude of 50 nm. Images of 512 × 512 pixels were acquired with the scan rate of 0.5 to 1 Hz. The force curves were analyzed using the NanoScope Analysis 1.50 software.

Reduced Young's Modulus (E^*) was estimated from the retract curve fit in the elastic regime[41] represented in green in the retraction force−distance curve (Figure 2) using the Derjaguin-Muller-Toporov model[42] shown in eq 2:

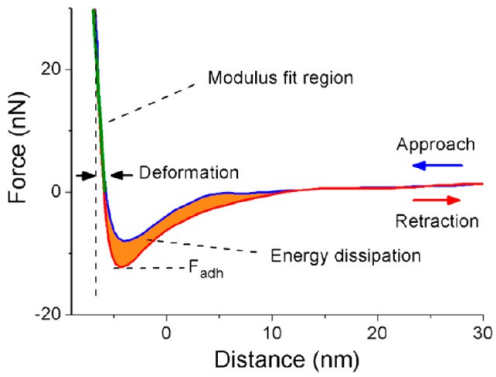

Figure 2. Force−distance curve for cured epoxy/eSIS/pCNT_0.1. Elastic modulus, adhesion force, and energy dissipation can be extracted from the force−distance curve. The adhesion force is the minimum of the retraction force−distance curve. Energy dissipation represents the orange shaded area between the approach and retraction force−distance curve.

$$F - F_{adh} = \frac{4}{3}E^*\sqrt{R(d - d_0)^3} \tag{2}$$

where $F - F_{adh}$ is the force on the cantilever relative to the adhesion force, R is the tip end radius, and $d - d_0$ is the deformation of the sample. The initial contact point where the tip starts to penetrate the sample was determined following a procedure described by Butt et al.[43]

Energy dissipation (E_{dis}) is given by the force times the velocity integrated over one period of the vibration (represented as the orange region in Figure 2) as in eq 3:

$$E_{dis} = \int_0^{z_{cycle}} F\,dZ = \int_0^T Fv\,dt \tag{3}$$

where (E_{dis}) represents dissipated energy per cycle of interaction, F is the interaction force vector, and dZ is the displacement vector. Since the velocity reverses its direction in approach and retract cycles, the integration is zero if the loading and unloading curves coincide. Energy

DOI: 10.1021/acsami.6b13212
ACS Appl. Mater. Interfaces 2017, 9, 930−943

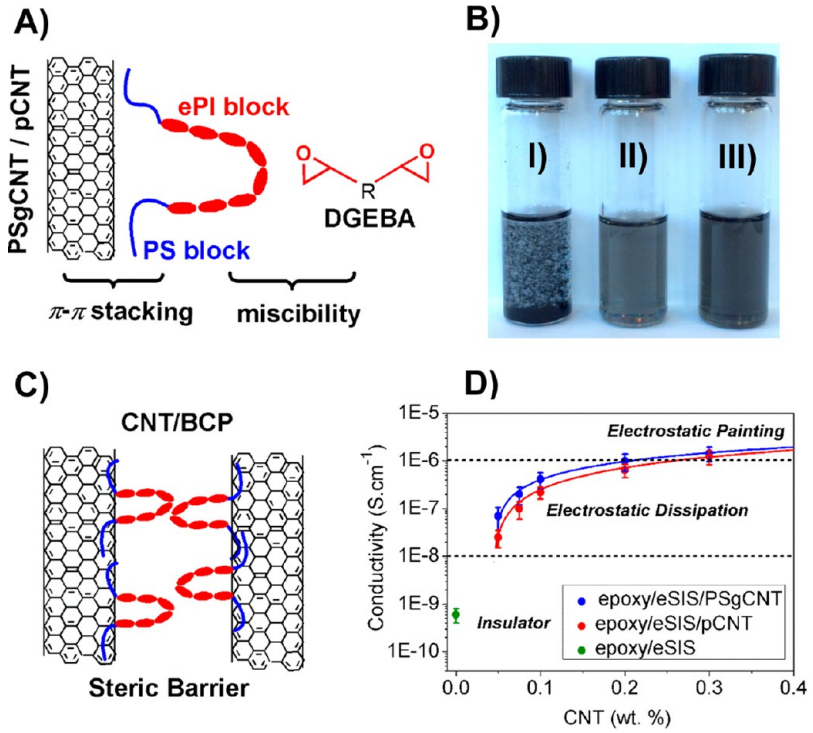

Figure 3. (A) Scheme of the proposed eSIS conformation, where PS block interacts with CNT walls by $\pi-\pi$ stacking and ePI block extends free into solution being miscible with DGEBA. (B) CNT dispersion photographs taken 15 min after the sonication step: (I) pCNT/eSIS in toluene/DT; (II) pCNT/eSIS in toluene/DT/DGEBA; (III) PSgCNT/eSIS in toluene/DT/DGEBA (CNT concentration: 0.025 mg/mL). (C) Scheme of steric barrier of eSIS limiting CNT/CNT contacts. (D) Bulk electrical conductivity for epoxy nanocomposites vs CNT content. Each data point reflects an average value based on three specimens, and the error bars indicate the standard deviation. Solid lines correspond to the fitting curves of the percolation model, and the dashed lines represent the lower limits of electrical conductivity required for the specified applications.[52]

dissipation is presented in electron volts as the mechanical energy lost per contact cycle.

Scanning Electron Microscopy (SEM). Scanning electron microscopy was performed using a scanning electron microscope (FEG-SEM Zeiss Supra 40) with an operative voltage of 5 kV for top and cross-sectional views and 3 kV for images taken on wear surfaces. SEM images were taken after platinum coating by sputtering.

Abrasion Tests. Nanocomposite abrasive measurements were performed by the ball cratering microscale-abrasive wear test proposed by Kassman et al.[44] The tests were conducted with a Calotest device.[45] A stainless steel ball (radius of 11 mm, weight of 44.8 g) was rolled against the specimens in the presence of fine alumina particles (diameter of 1−3 μm) under wet conditions. The geometry of the wear scar was assumed to reproduce the spherical geometry of the ball, and the wear volume (V) was calculated after measuring the crater diameter by optical microscopy according to eq 4:

$$V \approx \pi b^4/64R \quad (\text{for } b \ll R) \tag{4}$$

where R is the radius of the rolling sphere and b is the diameter of the wear scar produced on the initially flat surface on the sample. Wear coefficient (k) was calculated using a model[46] equivalent to Archard's equation[47] for sliding wear:

$$V = kSN \tag{5}$$

where S is the total sliding distance and N is the normal load on the contact. Relative speed at the nominal contact point was 0.56 m·s^{-1} (calculated for the ball geometry and an angular speed of 490 rpm). The normal load values were calculated as a function of the geometrical parameters and the ball weight following a previously reported procedure.[47] Five tests were completed for each nanocomposite for 1 min. All samples were cleaned with distilled water before optical microscopy and SEM characterization.

RESULTS AND DISCUSSION

Nanocomposite Preparation. A set of nanocomposite samples was prepared with a matrix material consisting of a commercial epoxy resin, utilized in the aeronautic industry, and two different nanoelements: (i) core−shell nanostructures obtained by microphase separation of poly(styrene-*b*-[isoprene-*ran*-epoxyisoprene]-*b*-styrene) (eSIS) block copolymer (10 wt %) within the epoxy thermoset and (ii) multiwalled carbon nanotubes. A set of CNT was subjected to polystyrene (PS) surface covalent functionalization (PSgCNT) while others were added without chemical functionalization (pCNT). The amount of CNT was varied in the range of 0.05−0.3 wt %. We specifically limited our analysis to relatively low loading fractions of CNT. Larger CNT loading fractions are impractical because of the prohibitive cost of CNT and additional care needed to achieve proper dispersion. It is well documented that mechanical properties of polymer nanocomposites reinforced with CNT are strongly dependent on the CNT dispersion state.[10] For this reason, it is essential to know the dispersion state of CNT to address a complete analysis of nanocomposite properties incorporating PSgCNT and pCNT and avoid misinterpretations by comparing materials that display different properties due to differences in CNT dispersion states. Therefore, carbon nanotubes (PSgCNT and pCNT) were dispersed by ultrasonic vibration in the presence of eSIS block copolymer using toluene/dodecanethiol/DGEBA mixtures as solvent. DT was used as cosolvent because it enables good and stable dispersions of PSgCNT upon sonication using toluene as solvent[30] which is interpreted in terms of the similar solubility parameters (δ) between PS (18.9 MPa$^{-1/2}$) and DT (19.1

DOI: 10.1021/acsami.6b13212
ACS Appl. Mater. Interfaces 2017, 9, 930−943

$MPa^{-1/2}$) calculated on the basis of the Hoftyzer and Van Krevelen theory.[48,49] Under the basis of the previous argument, we assume that DT is a good solvent for PS chains and therefore it aids solubility of PS grafted chains in PSgCNT upon sonication as well as increasing PS block solubility by the subsequent addition of eSIS to the CNT dispersion. In addition, DT is a low vapor pressure solvent (2.5 mmHg at 25 °C) that reduces toluene evaporation rate[35] and thus increases the mobility of BCP during self-assembly. In this regard, AFM phase imaging revealed that epoxy/eSIS films prepared with toluene as solvent (without DT) results in smaller sphere-like nanostructures (Supporting Information), while when using DT as cosolvent the BCP renders short cylinder-like nanostructures, presumably due to the higher mobility of eSIS during the self-assembly stage (before the solvent evaporation step under vacuum) enabling nanodomain association/aggregation.

Before the solvent evaporation step, it is likely that PS block interacts favorably with CNT walls by $\pi-\pi$ stacking,[50,51] while epoxidized polyisoprene (ePI) block extends free into solution due to the favorable interaction with DGEBA, as expected from the similar solubility parameters (δ_{ePI} = 20.3 $MPa^{-1/2}$; δ_{DGEBA} = 20.7 $MPa^{-1/2}$).[18] On the basis of the previous argument, Figure 3A depicts a possible conformation for eSIS consisting of PS blocks wrapping CNT walls and ePI subchains generating a steric barrier that prevents CNT agglomeration, in a similar way as previously reported by Kang and Taton for a polystyrene-*block*-poly(acrylic acid) BCP surrounding single-walled carbon nanotubes dispersed in water.[14] To give evidence of such BCP assisted dispersion of CNT, we studied CNT stability in the presence of eSIS using a toluene/DT or toluene/DT/DGEBA mixture as solvent. A toluene/DT solvent mixture (135/5.5; v/v) results in the formation of a pCNT precipitate shortly after ultrasonic vibration (Figure 3BI), due to the absence of the stabilizing interaction between ePI blocks and DGEBA. On the contrary, when epoxy monomer DGEBA is added to the same solvent system, no precipitation (pCNT or PSgCNT) is observed, supporting the assumption that eSIS aids CNT dispersion, as presented in Figure 3BII,III. Increased solubility of the ePI block in the toluene/DT/DGEBA mixture compared to toluene/DT as the solvent system is likely to be responsible for the significant change in CNT dispersion stability, enabling the ePI block to generate a steric barrier that limits CNT contacts, as sketched in Figure 3C. Characterization of CNT dispersion state in the cured epoxy nanocomposite films was conducted by measuring bulk electrical conductivity of the obtained nanocomposites bearing pCNT and PSgCNT in the range of 0.05−0.3 wt %. Figure 3D shows the effect of pCNT and PSgCNT content on the electrical conductivity. The electrical conductivity of epoxy nanocomposites shows a typical percolation behavior indicating formation of a conductive network above a critical concentration, defining the percolation threshold.

Percolation threshold can be interpreted as an indication of CNT dispersion degree in epoxies[53] and was therefore obtained by plotting the electrical conductivity as a function of the nanofiller content (wt %) and fitting with a power law relationship as follows:

$$\sigma = \sigma_0(\varnothing - \varnothing_C)^t \quad (6)$$

where σ_0 is the maximum observed conductivity, $\varnothing$ is CNT content (wt %), $\varnothing_C$ is the electrical percolation threshold, and t is the factor form parameter. The fitting parameters are presented in Table 1. The percolation threshold obtained for nanocomposites containing pCNT ($\varnothing_C$ = 0.047 wt %) and PSgCNT ($\varnothing_C$ = 0.045 wt %) shows no significant differences, suggesting a similar CNT dispersion degree for nanocomposites prepared with pCNT and PSgCNT. Even though grafted PS chains in PSgCNT walls may improve CNT dispersion compared to pCNT in organic solvents and polymeric matrices,[30] it is evidenced that the dominant factor contributing to CNT dispersion is noncovalent functionalization by BCP. In fact, if PS grafted chains in PSgCNT are not highly solvated in the solvent system toluene/DT/DGEBA, the effect of additional steric barriers provided by PS grafted in PSgCNT would be negligible.

Table 1. Percolation Model Fitting Parameters for Electrical Conductivity

CNT	σ_0 (10^{-6} S·cm^{-1})	$\varnothing_C$ (wt %)	t	R^2
pCNT	5.0 ± 0.4	0.047 ± 0.004	1.06 ± 0.06	0.9945
PSgCNT	4.7 ± 0.4	0.045 ± 0.005	0.85 ± 0.07	0.9957

The curing process of the DGEBA/ancamine system modified with eSIS has been extensively investigated in previous articles.[19,30,32] Dynamic DSC experiments were conducted to determine the glass transition temperature of cured samples. Table 2 displays the T_g values obtained for cured epoxy nanocomposites together with the T_g values for cured epoxy and eSIS for comparative purposes. Heat capacity change (ΔC_p) values at each T_g are also provided in Table 2 as a measure of the amount of amorphous phases at each transition. Epoxy nanocomposites present three glass transition temperatures. A major T_g at ∼110 °C is attributed to the epoxy rich phase modified by interpenetrated ePI subchains. This glass transition temperature taken from the first and second heating scan does not show significant differences, suggesting complete curing. It is evidenced that incorporating ePI subchains in the epoxy matrix results in a glass transition temperature upshift in the range of 18−23 °C, in agreement with previous T_g results of nanostructured epoxy thermosets containing 10 wt % of poly(dimethylsiloxane)−poly(glycidyl methacrylate).[54] Such antiplasticizing effect is presumably a consequence of ePI subchains interpenetrating the epoxy matrix and occupying a matrix free volume. Table 2 also shows a T_g at ∼8 °C close to ePI T_g in neat eSIS (∼10 °C), suggesting that a certain proportion of ePI subchains is demixed from the epoxy matrix under the basis of a polymerization induced microphase separation mechanism.[32] A third minor T_g is between 64 and 72 °C, attributed to the minority PS rich phase (∼3 wt %). It is evidenced that the T_g of PS phase for epoxy/eSIS (64 °C) is well below the reference value of PS T_g (72 °C for neat eSIS), which was measured directly from a bulk eSIS sample not dissolved in the toluene/DT solvent system. Therefore, the observed discrepancy could be ascribed to residual solvent traces after the evaporation step in epoxy/eSIS. However, this effect is only observed for PS phase T_g, suggesting that DT traces may selectively remain within the PS nanodomains. It is worth noting that PS phase T_g clearly increases with respect to the value observed for epoxy/eSIS by the incorporation of PSgCNT or pCNT, which is likely due to the stiffening of PS segments caused by CNT/PS phase interactions.[55] On the contrary, no significant differences are found in ePI and epoxy matrix rich T_g values by the incorporation of PSgCNT or pCNT.

DOI: 10.1021/acsami.6b13212
ACS Appl. Mater. Interfaces 2017, 9, 930−943

Table 2. Glass Transition Temperatures of Cured Epoxy, eSIS, and Cured Epoxy Nanocomposites

	glass transition temperature (°C); [ΔC_p] (J/g °C)			
			epoxy matrix	
material	ePI	PS	1st heating scan	2nd heating scan
epoxy			89 ± 1	90 ± 2; [0.367]
eSIS	10 ± 2; [0.343]	72 ± 3; [0.102]		
epoxy/eSIS	8 ± 2; [0.021]	64 ± 3; [0.020]	107 ± 2	110 ± 3; [0.233]
epoxy/eSIS/PSgCNT_0.1	9 ± 2; [0.025]	70 ± 3; [0.020]	109 ± 3	113 ± 3; [0.242]
epoxy/eSIS/PSgCNT_0.3	8 ± 2; [0.028]	72 ± 3; [0.024]	105 ± 3	108 ± 3; [0.241]
epoxy/eSIS/pCNT_0.3	9 ± 2; [0.025]	71 ± 3; [0.023]	106 ± 3	110 ± 3; [0.241]

Reduced Young's Modulus of nanocomposites at room temperature are compared to that for neat epoxy matrix, as presented in Figure 4. Neat epoxy E^* is determined to be 2.40 GPa. E^* is related to the Young's Modulus of the sample (E_s) by eq 7:[39]

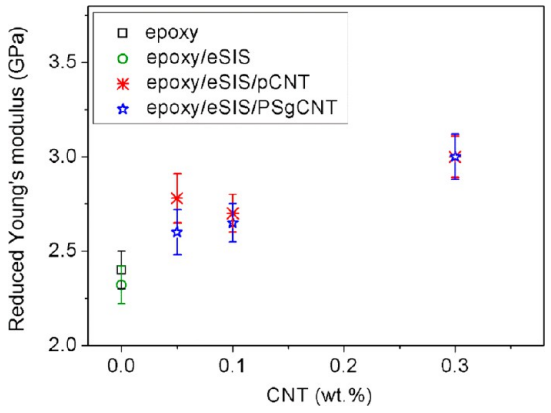

Figure 4. Reduced Young's Modulus for cured epoxy, epoxy/eSIS, and the different nanocomposites obtained from the retraction curve fit using the Derjaguin-Muller-Toporov model.

$$E^* = \left[\frac{1-\nu_s^2}{E_s} + \frac{1-\nu_{tip}^2}{E_{tip}}\right]^{-1} \quad (7)$$

where E_{tip} is the tip modulus and ν_s and ν_{tip} are the sample and tip Poisson's ratio, respectively. Assuming a Poisson's ratio of 0.3 for neat epoxy and that E_{tip} is infinite, the epoxy Young's Modulus is calculated to be 2.6 GPa, which corresponds well (within experimental error) with neat epoxy elastic modulus obtained from dynamic mechanical analysis (3.0 GPa) (data not shown). Incorporation of 10 wt % of eSIS does not show significant differences in reduced Young's Modulus, while the addition of CNT results in an improvement in E^* of ~25% for both types of CNT at the highest loading CNT loading (0.3 wt %), in agreement with the expected trend in epoxy Young's Modulus reinforced with CNT.[56,57]

Morphology. Nanocomposite nanostructure at the polymer/air interface was investigated by AFM and SEM measurements. Figure 5 shows representative AFM phase and tip−sample adhesion images of epoxy nanocomposites with different CNT concentrations. It is evidenced that eSIS displays an irregular nanostructure pattern regardless of the PSgCNT content as presented in Figure 5A,C for 0.05 and 0.3 wt % of PSgCNT, respectively. The brighter features are identified as the BCP nanodomains, and the dark regions correspond to the epoxy matrix according to the epoxy/BCP blending composition in the nanocomposites (≈90/10 wt %). The same irregular pattern was observed by SEM-top imaging collected after Pt sputtering, as presented in Figure 5B for epoxy/eSIS/PSgCNT_0.5. A remarkable feature of eSIS nanostructuration within the epoxy thermoset was evidenced by adhesion imaging, resolving the core (dark) and shell (bright) nanodomain regions characterized by different adhesion forces between sample and tip, as shown in Figure 5C for epoxy/eSIS/PSgCNT_0.3. These structures resemble a dispersion of short cylinders perpendicular to the surface that expose their cores to the polymer/air interface. We assign dark cores (lowest tip−sample adhesion regions) to PS nanodomains, which self-assemble before the curing process due to the lack of compatibility with the epoxy precursors.[32] On the other hand, the brighter shell regions, surrounding the dark nanodomains, are attributed to ePI rich nanodomains. However, it is not clear if these regions are related to (i) the ePI rich phase demixed from the epoxy matrix, according to the presence of a T_g ~ 10 °C in DSC thermograms; (ii) the ePI rich phase interpenetrating and cross-linked to the epoxy matrix; or (iii) a combination of both.

Another interesting aspect evidenced by AFM PeakForce adhesion map in Figure 5D is that the core−shell structures are not isolated but interconnected/aggregated to some extent. This observation is in agreement with the short and irregular patterns described from AFM phase image and SEM top-image analysis, although the latter techniques did not resolve the inner structure of the nanodomains. Previous articles investigating the type of BPC core−shell morphology within epoxy thermosets were generally conducted by transmission electron microscopy of thin specimens obtained from bulk cured samples.[20,58] However, it is worth noting that the latter approach is not feasible to characterize the polymer/air interface of a thin epoxy coating.

Surface characterization by SEM and AFM imaging does not reveal isolated or CNT bundles, which may be attributed to the rather low CNT concentration in the nanocomposites. In this regard, Karippal et al. characterized epoxy/CNT composites by AFM phase imaging and identified CNT as bright spots and tubular structures, however at much higher CNT contents of between 5 and 10 wt %.[59]

In order to gain more insight on the nanoelements integration within the epoxy films, cross-sectional SEM images of cured nanocomposites are presented in Figure 6. Figure 6A−C displays cross-sectional views of epoxy/eSIS/PSgCNT_0.3 nanocomposite showing short irregular nanostructures aggregated to some extent, which we attribute to BCP domains. These structures are distributed through the entire film thickness (Figure 6A) and have an average length of 48 ± 8 nm, consistent with the domain dimensions evidenced by AFM and SEM characterization shown in Figure 5. Although the

DOI: 10.1021/acsami.6b13212
ACS Appl. Mater. Interfaces 2017, 9, 930−943

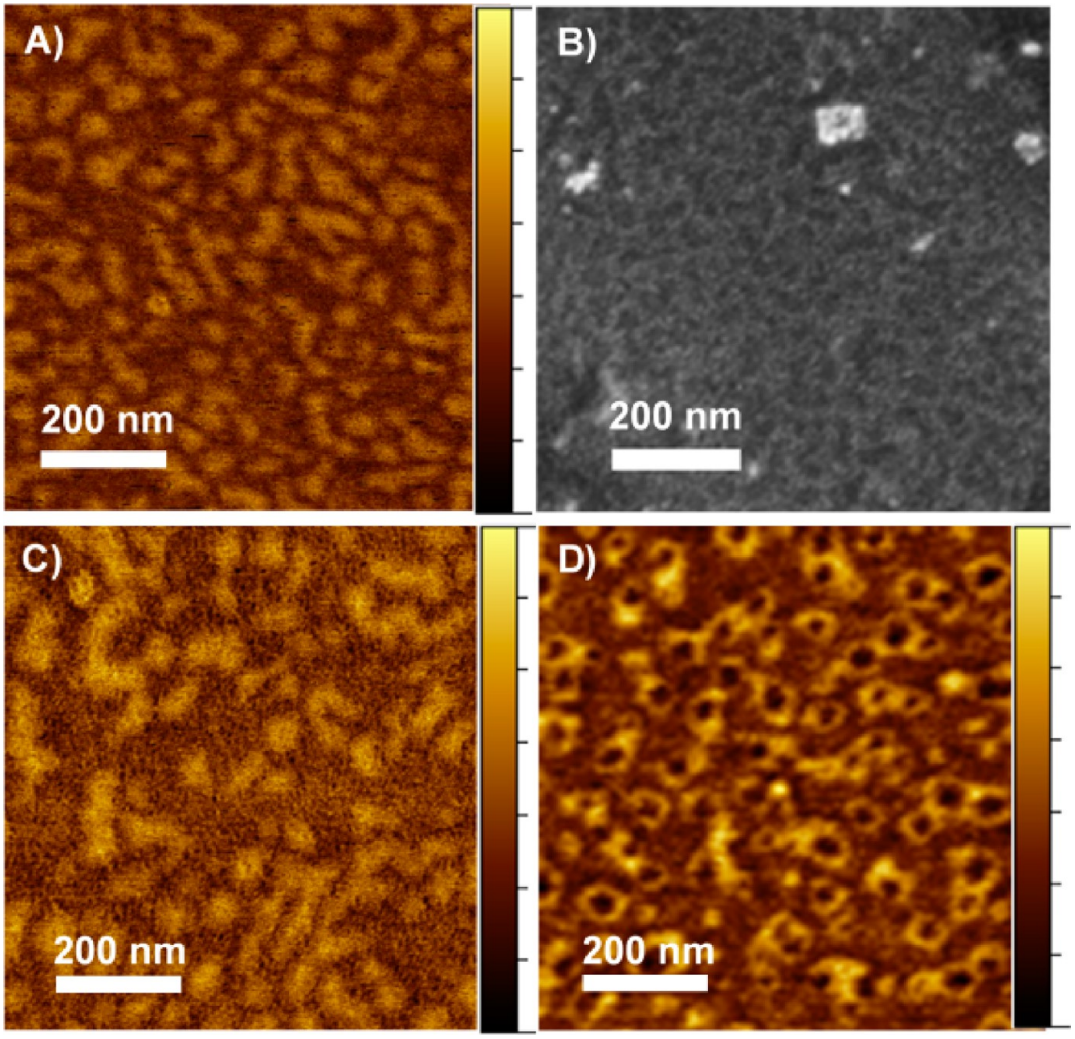

Figure 5. AFM tapping mode phase image (A) and SEM top-image (B) taken from epoxy/eSIS/PSgCNT_0.05. AFM tapping mode phase image (C) and AFM PeakForce adhesion map (D) taken from epoxy/eSIS/PSgCNT_0.3. Color scales correspond to 2−7° (A, C) and 0−7 nN (D).

inner structure of BCP domains is not resolved by SEM images, we assume the same core−shell morphology as evidenced by AFM characterization. CNT appeared as bright spots or tubular structures in SEM cross-sectional images with no sign of agglomeration, as presented in Figure 6B−D. Notably, CNT appear to be associated with BCP domains, as indicated by the arrows in Figure 6B−D, suggesting the formation of CNT−BCP conjugate structures as sketched in Figure 6E.

Potential explanations for this observation include: (i) CNT segregation to the PS/ePI interface of the BCP as reported by Arras et al. for pristine CNT and poly(styrene)-*b*-poly(2-vinylpyridine) micelles;[60] (ii) co-assembly of eSIS chains around CNT walls by noncovalent functionalization, as demonstrated in solutions of CNT and amphiphilic BCP bearing at least one block capable of forming a close interaction (for example, $\pi-\pi$ interaction)[21,23] with the CNT walls.

Given that cross-sectional SEM images do not resolve the inner structure of BCP domains within cured nanocomposites, concluding about which mechanism originates CNT−BCP conjugates remains elusive. However, we note that coassembly of BCP chains and CNT would be favored by $\pi-\pi$ interaction between phenyl groups of PS blocks and the extended π-system of CNT, replacing to some extent the rather poor wetting of CNT with epoxy.[61]

The formation of CNT−BCP conjugate structures is consistent with the ultrasound-assisted noncovalent functionalization of CNT by eSIS during the nanocomposite preparation protocol and with the increase of PS phase T_g by the incorporation of CNT, suggesting CNT−PS phase interactions. We also suggest that, for the case of PSgCNT−BCP conjugate, PS grafted chains of PSgCNT could selectively localize within the adjacent PS phase of BCP in a similar way as described by Li et al. for a system consisting of single walled carbon nanotubes covalently functionalized with poly(*N*,*N*-dimethylacrylamide)-*b*-poly(*N*-isopropylacrylamide-*co*-*N*-acryloxysuccinimide) (PDMA-*b*-P(NIPAM-*co*-NAS) chains blended with identical PDMA-*b*-P(NIPAM-*co*-NAS) free chains.[22]

Given that energy dissipation capability of epoxy coatings is a key aspect for assessing material durability, we systematically studied nanocomposite energy dissipation by PeakForce QNM and wear coefficient by abrasion tests in order to evaluate the potential of CNT−BCP conjugates as mechanical reinforcement for epoxy coatings.

Energy Dissipation. Figure 7A displays representative force versus distance curves for the epoxy system (I), epoxy/eSIS/pCNT_0.3 (II), and epoxy/eSIS/PSgCNT_0.3 (III). The obtained force−distance curves are characteristic of deformable materials with attraction and adhesion force displaying

DOI: 10.1021/acsami.6b13212
ACS Appl. Mater. Interfaces 2017, 9, 930−943

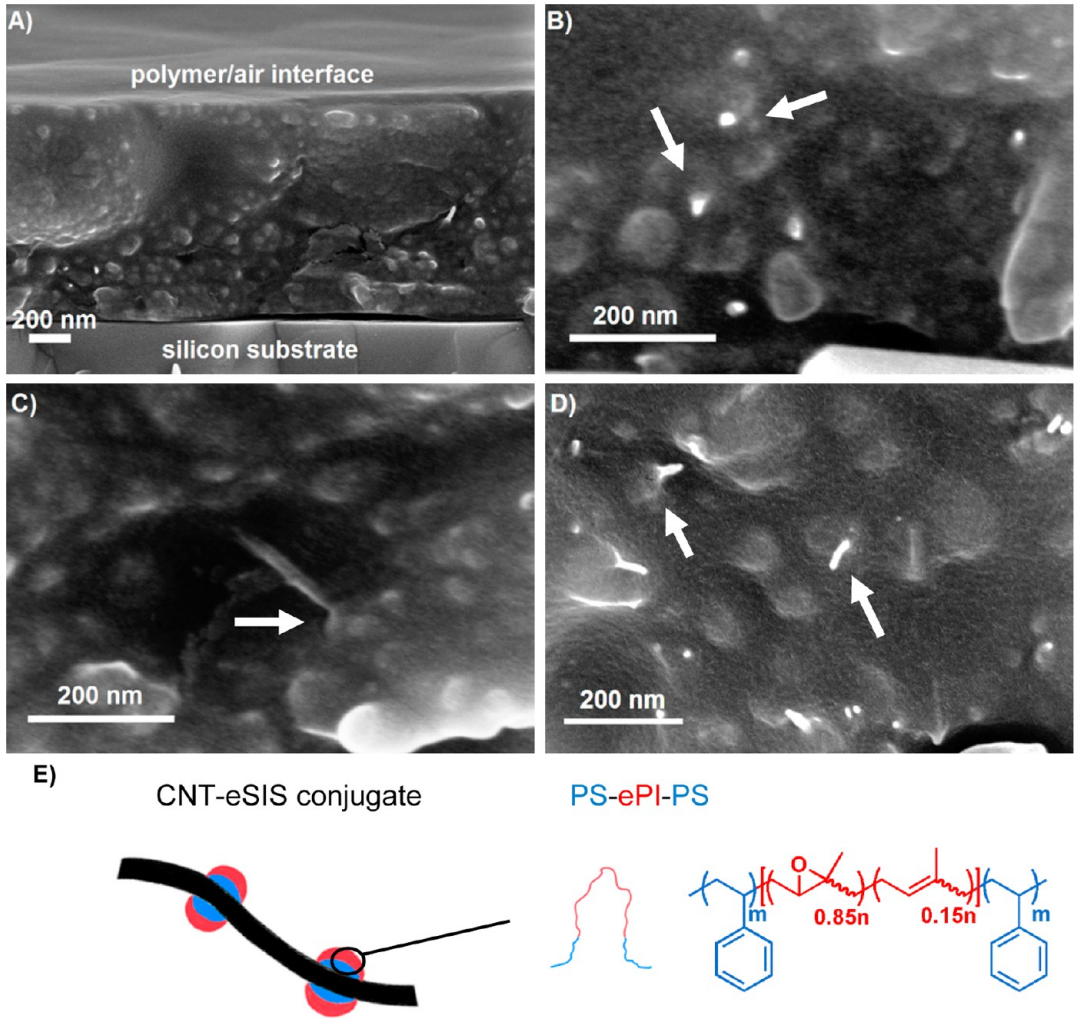

Figure 6. SEM cross-sectional views taken from epoxy/eSIS/PSgCNT_0.3 (A–C) and epoxy/eSIS/pCNT_0.3 (D). Arrows indicate CNT–BCP coassembly. (E) Schematic representation of CNT–BCP conjugate.

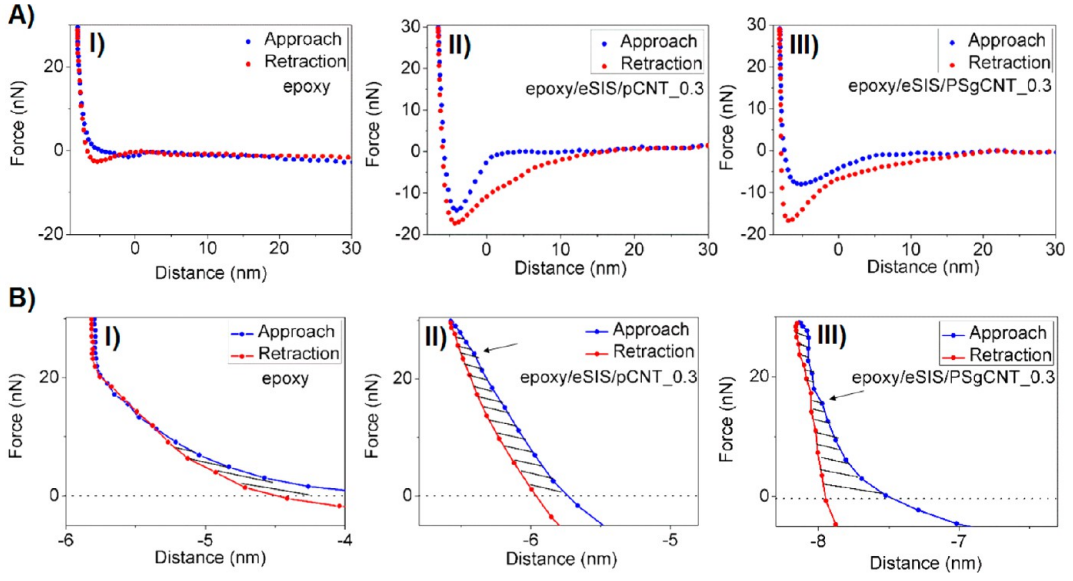

Figure 7. (A) Representative force versus distance curves for neat epoxy (I), epoxy/BCP/pCNT_0.3 (II), epoxy/BCP/PSgCNT_0.3 (III). (B) Representative force versus distance curves in contact region for neat epoxy (I), epoxy/eSIS/pCNT_0.3 (II), and epoxy/eSIS/PSgCNT_0.3 (III). Arrows indicate yielding point in the approaching curve of the contact cycle. Shaded areas represent a measure of the energy needed for the deformation and dissipated into the sample.

DOI: 10.1021/acsami.6b13212
ACS Appl. Mater. Interfaces 2017, 9, 930–943

approach and retraction curves of the contact cycle that are not identical.[43] For such materials, attractive forces and adhesion can be a source of error in the determination of sample/stylus zero distance.[43,62] Therefore, stylus/sample zero distance was estimated for all samples as the midpoint between the onset and end of the jump-in in the approaching part of the cycle.[43] Negative distance in force−distance curves corresponds to indentation depth, being in the range of 6−8 nm ($\leq R$) at the maximum applied force (30 nN) for all samples.

The area difference between the approach and the retraction parts of each cycle represents total energy dissipation (E_{Dis}) per contact cycle.[43,62] E_{Dis} was calculated for neat epoxy and epoxy nanocomposites (Supporting Information). Energy dissipation per contact cycle trend could not be directly attributed to energy dissipation performance because work of adhesion is also involved in the total energy dissipation. In fact, adhesion force, defined as the cantilever pull-off force in the retraction part of the cycle, changed by incorporating BCP and CNT due to different sample−stylus surface interactions (surface effect). An alternative procedure to extract nanomechanical information for this type of material, avoiding the contribution of work of adhesion to energy dissipation, was reported by Butt et al.[43] The approach consists of analyzing force−distance curves in the contact regime, where the approach and retraction curves are not affected by work of adhesion. Figure 7B presents representative zoomed views of force−distance curves in the contact regime for neat epoxy (I), epoxy/eSIS/pCNT_0.3 (II), and epoxy/eSIS/PSgCNT_0.3 (III). For all samples, the approach and withdrawal contact lines do not overlap, which indicates that plastic deformation occurs during nanoindentation.[43] In fact, the approach contact line for epoxy/eSIS/pCNT_0.3 (Figure 7BII) and epoxy/eSIS/PSgCNT_0.3 (Figure 7BIII) shows yielding points characteristic of plastic deformation, as indicated by the arrows in Figure 7BII,III.[43] The area between the two contact lines above the axis force = 0 (shaded areas in Figure 7B) represents the energy needed for the deformation and dissipated into the sample per contact cycle.[43]

Figure 8 presents the energy dissipated into deformations per contact cycle for the nanocomposites. E_{Dis} for neat epoxy and epoxy/eSIS are also included in Figure 8 for comparative purposes. Neat epoxy displays the lowest dissipated energy per contact cycle (11 ± 2 eV). Incorporation of BCP within the epoxy matrix results in a significant improvement of 120% in E_{Dis} in the contact regime compared to neat epoxy, in agreement with previous publications reporting increments in strain energy release of ∼100−200% for an epoxy matrix modified with 5 wt % of a polystyrene-*b*-poly(ethylene oxide) BCP forming glassy core micelles compared to neat epoxy.[63] By incorporating pCNT in the range of 0.05−0.3 wt %, dissipated energy further increases up to 4.3 times more than E_{Dis} for neat epoxy. Remarkably, this effect is even more pronounced for nanocomposites containing PSgCNT, with as much as 7.1-fold increase in dissipated energy in contact regime at 0.3 wt % loading of PSgCNT. This result is comparable to the exceptional increments in strain energy release (up to ∼6.3-fold with respect to neat epoxy) reported by Li et al. for an epoxy matrix modified with 5 wt % of poly(ethylene oxide)-*b*-poly(butylene oxide) BCP forming nanodomains with rubbery cores and glassy shells.[29] However, the latter system showed a 10% decrease in Young's Modulus with respect to neat epoxy. It is worth mentioning that the energy dissipation performance for all nanocomposites bearing different amounts of CNT is greater than the maximum toughness increment (∼65% with respect to neat epoxy) previously reported by incorporating CNT (0.5 wt %) functionalized with chemical groups capable of reacting with the epoxy precursors at the curing stage.[57] In addition, the increments in energy dissipation observed in this work largely exceed toughness improvements (∼270% with respect to neat epoxy) for an epoxy system comprising SWCNT (0.5 wt %) and 0.15 wt % of pluronic BCP used as surfactant.[56]

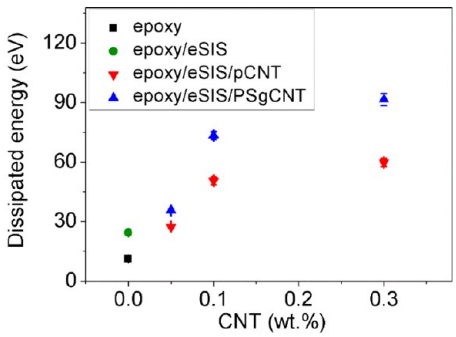

Figure 8. Energy dissipated during plastic deformation in the contact regime of force−distance curves. Each data point reflects an average value based on ten contact cycles, and the error bars indicate the standard deviation.

Wear Tests. To further examine the effect of CNT, BCP, and CNT−BCP conjugates on cured epoxy nanocomposite mechanical properties, mechanical degradation was performed by means of abrasion tests under wet conditions. Figure 9 shows wear coefficient (k) of cured neat epoxy and epoxy nanocomposites. Incorporation of both nanoelements to the epoxy matrix results in a different wear behavior. Incorporation of 10 wt % of BCP exerts great influence on wear resistance, as reflected by a 190% increase of wear coefficient with respect to that for neat epoxy, making the material more prone to mechanical degradation, in agreement with a previous publication by Esposito et al. for an epoxy matrix modified with epoxidized poly(styrene-*b*-butadiene-*b*-styrene).[26] On the other hand, wear coefficient decreases with CNT content with a k value for epoxy/eSIS/PSgCNT_0.3 being 17% lower than that for neat epoxy.

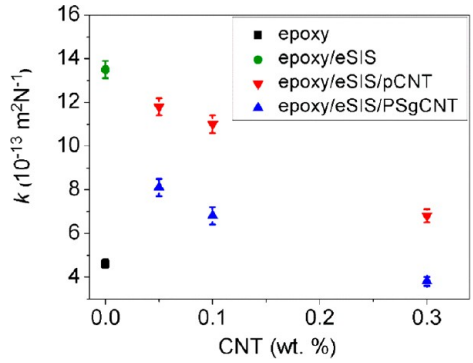

Figure 9. Wear coefficient (k) as a function of CNT loading. Neat epoxy and epoxy/eSIS values are represented in black and green, respectively. Each data point reflects an average value based on five specimens, and the error bars indicate the standard deviation.

DOI: 10.1021/acsami.6b13212
ACS Appl. Mater. Interfaces 2017, 9, 930−943

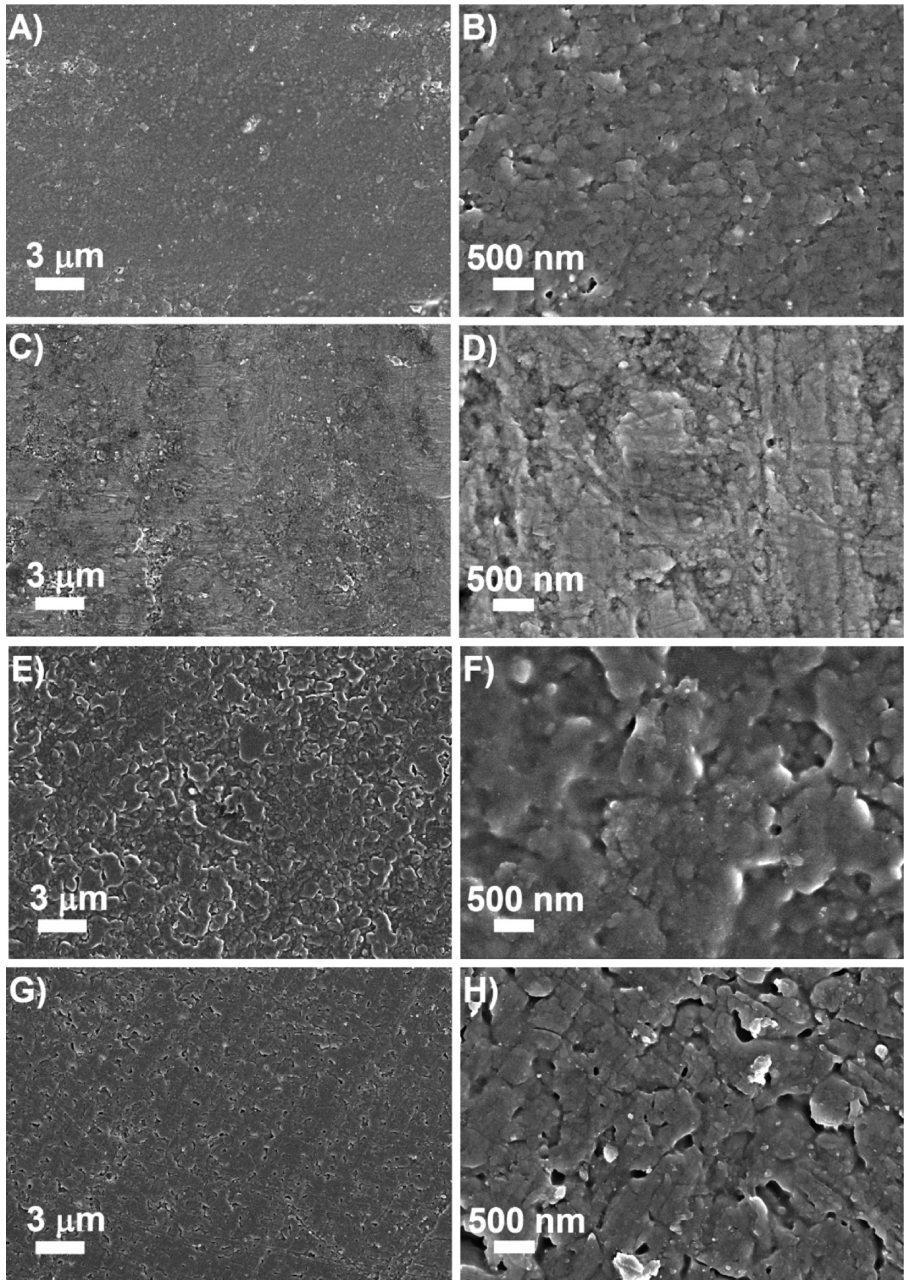

Figure 10. SEM top-images taken on wear surfaces for neat epoxy (A, B), epoxy/eSIS (C, D), epoxy/eSIS/PSgCNT_0.3 (E, F), and epoxy/eSIS/pCNT_0.3 (G, H).

In this regard, previous work reported similar trends in wear coefficients by incorporating CNT to an epoxy matrix in the range of 0.1 to 0.5 wt %.[64] Moreover, Figure 9 suggests that the actual wear mechanism strongly depends on the type of CNT incorporated to the nanocomposite and thus on the type of CNT−BCP conjugate that is formed. It was found that nanocomposites prepared with PSgCNT are less prone to mechanical degradation than those incorporating the same pCNT content. Since nanocomposites incorporating PSgCNT presented higher energy dissipation performance and lower wear coefficient than pCNT counterparts, it seems that nanocomposites with higher energy dissipation properties are able to absorb more shear energy before fracture and therefore exhibit less mass loss overall during wear tests than composites containing pCNT.

Wear behavior depends on many properties such as hardness, fracture toughness, friction, extensibility, and the hardness and size of the released particles.[65] Lee developed a simplified relationship of the abrasive wear resistance and the fracture energetics for brittle polymers, as follows:[66]

$$V = k'\left(\frac{\sigma_y \gamma^{3/2}}{G_{1C} H^{3/2}}\right) S \tag{8}$$

where V is the wear volume (proportional to k), k' is a constant, S is the sliding distance, σ_y is the yield strength, γ is the surface energy, H is the indentation hardness, and G_{1C} is the mode I fracture energy release rate. We assume that eq 8 can be used for epoxy-based systems modified with 10 wt % of eSIS and low contents of CNT (up to 0.3 wt % or ∼0.26 vol

DOI: 10.1021/acsami.6b13212
ACS Appl. Mater. Interfaces 2017, 9, 930−943

%). Moreover, considering the low CNT content and the similar surface energy values for epoxy, PS, and ePI ($\gamma_{epoxy} \sim 44$ mJ/m^2; $\gamma_{PS} = 40.7$ mJ/m^2; $\gamma_{ePI} \sim 41.9$ mJ/m^2), the surface energy can be assumed to remain constant for the different nanocomposites.[67,68] The observed trend in wear coefficient for the nanocomposites is interpreted as a result of the combined increase in energy dissipation and hardness[69] as the CNT concentration increases compared to that for epoxy/eSIS, while the yield strength slightly decreases with CNT addition, as deduced from yielding points in force−distance curves. Furthermore, Zhang et al. suggested that, when CNT are exposed to the sliding interface, substantial CNT deformation and fragmentation can occur resulting in a protective effect on the epoxy matrix wear behavior.[70]

In order to get a more detailed picture into the nanocomposites behavior under mechanical abrasion, wear microstructures of abraded specimens were examined by SEM. Representative SEM micrographs of wear surfaces are presented in Figure 10. Neat epoxy sample shows a relatively smooth surface with some fine texture in the range of 300 nm (Figure 10A,B). By incorporating BCP (10 wt %) (Figure 10C,D), the wear microstructure displays a rougher surface with a more irregular texture with sizes in the range of 300 to 500 nm (Figure 10D), suggesting that soft nanoinclusions increase the tendency of the material to produce local deformations under shear energy. Figure 10E,F displays epoxy/eSIS/PSgCNT_0.3 microstructure after mechanical degradation. Interestingly, it is evidenced that wear surface displays a much rougher pattern, with irregular holes with sizes in the range of 750 to 1200 nm, as a result of more local deformation in response to shear stress. Such pattern clearly differs from that encountered in the wear surface of epoxy/eSIS/pCNT_0.3, which exhibits irregular cavities and local deformations with smaller sizes in the range of 300 to 600 nm.

Taken together, the above results of energy dissipation and wear abrasion tests provide strong evidence that the coassembly of CNT−BCP conjugate plays a key role in energy dissipation mechanisms of the nanocomposites. Slippage was suggested as the mechanism responsible for the enhancement of strain energy dissipation in polymer/CNT composites.[28] The slip mechanism consists of energy dissipation by frictional sliding that occurs at the interface between matrix and reinforcement. Gardea et al. investigated the slip mechanism in a composite material consisting of a polystyrene matrix with aligned single-walled carbon nanotubes (1 wt %). Compared with neat PS matrix, there was an increase of as much as 100% in energy dissipation by the incorporation of CNT.[28] On the other hand, Bates and co-workers highlighted that the main energy absorbing processes in epoxies modified by BCP nanodomains are those that promote shear yielding and plastic deformation triggered by epoxy network disruption caused by the corona chains (ePI subchains for the system studied here).[29,63]

Therefore, in the nanocomposites of the present study, it is likely that a large number of mechanisms operate simultaneously in energy dissipation[27] such as slip at the matrix−CNT interface, plastic deformation of BCP nanodomains which facilitates epoxy matrix shear yielding, and plastic deformation triggered by epoxy network disruption caused by BCP nanodomains. In this regard, formation of CNT−BCP conjugates, as revealed by SEM cross-sectional imaging of nanocomposites, could increase the load transfer between CNT and the matrix under strain. Therefore, upon relative displacement between CNT and the matrix (slip), mechanical interlocking provided by CNT−BCP conjugates will give rise to frictional components for energy dissipation, contributing to the global energy dissipation mechanism. One explanation for the greatest improvement in energy dissipation observed in epoxy nanocomposites incorporating PSgCNT and eSIS with respect to pCNT and eSIS would be that PS grafted chains of PSgCNT possibly localize into the PS cores of adjacent eSIS nanodomains under the basis of selective confinement[31] providing physical links between the CNT and BCP nanodomains. We speculate that such interconnection between the high aspect ratio PSgCNT and eSIS nanodomains provides a means to amplify the triggering events for energy dissipation that occur by epoxy network disruption caused by interpenetrated ePI subchains within the matrix. The latter scenario would not be operative for the nanocomposites incorporating purified CNT and BCP due to the absence of such interconnected nanoassemblies. Future work will be devoted to confirm the extent of the above-mentioned energy dissipation mechanisms in the nanocomposites of the present study.

CONCLUSION

We have developed thin epoxy coatings reinforced with carbon nanotubes and eSIS block copolymer that coassemble into CNT−BCP conjugate structures by an ultrasound-assisted noncovalent functionalization process. The association of CNT and BCP nanodomains is suggested by cross-sectional SEM images of cured nanocomposites, by the assisted dispersion of CNT by the block copolymer chains and by an increase in PS phase T_g with the addition of CNT compared to that for the epoxy matrix modified with BCP.

Nanocomposites prepared with PSgCNT and eSIS display higher energy dissipation performance than those containing pCNT and eSIS, with a remarkable enhancement in energy dissipation of up to 7.1-fold with respect to neat epoxy at a PSgCNT load of 0.3%. This outstanding result is comparable to the increment in strain energy release reported for an epoxy system modified with BCP micelles with rubbery cores and glassy shells.[29] However, the latter system showed a 10% decrease in Young's Modulus while the nanocomposites of the present study show an increase in this property of up to 25% compared to the neat epoxy. Energy dissipation performance is also reflected by a marked decrease of wear coefficient for materials bearing PSgCNT than those incorporating pCNT, with a reduction of wear coefficient as much as 17% with respect to neat epoxy. Moreover, SEM imaging on wear surfaces reveals that addition of PSgCNT and BCP results in a material capable of absorbing more shear energy into deformations before particle release. The relative enhancement of energy dissipation performance between nanocomposites prepared with PSgCNT−BCP and pCNT−BCP is proposed to arise from hierarchical assembly of PS grafts in PSgCNT and PS core of eSIS nanodomains, providing additional frictional components for energy dissipation through the slip mechanism and favoring material deformation. This work highlights the significance of CNT−epoxy interface engineering for enhancing the mechanics of epoxy coatings.

ASSOCIATED CONTENT

Supporting Information

The Supporting Information is available free of charge on the ACS Publications website at DOI: 10.1021/acsami.6b13212.

DOI: 10.1021/acsami.6b13212
ACS Appl. Mater. Interfaces 2017, 9, 930−943

Gel permeation chromatography traces for SIS and eSIS; isothermal and dynamic DSC traces for the DGEBA/ancamine system; AFM phase image of epoxy/eSIS prepared in the absence of DT; total energy dissipation per contact cycle for neat epoxy and epoxy nanocomposites (PDF)

AUTHOR INFORMATION

Corresponding Authors

*E-mail: hernan.garate@cea.fr.
*E-mail: norma@qo.fcen.uba.ar.

ORCID

Hernan Garate: 0000-0002-7723-1013

Present Address

¶H.G.: LIONS, NIMBE, CEA, CNRS, Université Paris-Saclay, CEA-Saclay, 91191 CEDEX Gif-sur-Yvette, France.

Notes

The authors declare no competing financial interest.

ACKNOWLEDGMENTS

The authors are thankful for financial support from UBACyT (Nos. 20020120100155BA, 20020130100495BA, and 20020130100021BA); ANPCyT (PICT-2012-0717 and PICT-2012-1093); CONICET (PIP 2013-2015 11220120100508CO, 11220110100370CO). H.G. and M.B. also acknowledge CONICET for their doctoral fellowships. The authors are also thankful for funding from the European Community (POCO Project, 7th Framework Programme, NMP-213939).

REFERENCES

(1) Baur, J.; Silverman, E. Challenges and Opportunities in Multifunctional Nanocomposite Structures for Aerospace Applications. *MRS Bull.* **2007**, *32*, 328−334.

(2) Li, Q.; Chen, L.; Gadinski, R.; Zhang, S.; Zhang, G.; Li, H. L.; Iagodkine, E.; Haque, A.; Chen, L.-Q.; Jackson, T. N.; Wang, Q. Flexible High-Temperature Dielectric Materials from Polymer Nanocomposites. *Nature* **2015**, *523*, 576−579.

(3) Jancar, J.; Douglas, J. F.; Starr, F. W.; Kumar, S. K.; Cassagnau, P.; Lesser, A. J.; Sternstein, S. S.; Buehler, M. J. Current Issues in Research on Structure-Property Relationships in Polymer Nanocomposites. *Polymer* **2010**, *51*, 3321−3343.

(4) Kang, Y. J.; Chun, S.-J.; Lee, S.-S.; Kim, B.-Y.; Kim, K. H.; Chung, H.; Lee, S.-Y.; Kim, W. All-Solid-State Flexible Supercapacitors Fabricated with Bacterial Nanocellulose Papers, Carbon Nanotubes, and Triblock-Copolymer Ion Gels. *ACS Nano* **2012**, *6*, 6400−6406.

(5) Choi, J. R.; Yu, S.; Jung, H.; Hwang, S. K.; Kim, R. H.; Song, G.; Cho, S. H.; Bae, I.; Hong, S. M.; Koo, C. M.; Park, C. Self-Assembled Block Copolymer Micelles with Silver-Carbon Nanotube Hybrid Fillers for High Performance Thermal Conduction. *Nanoscale* **2015**, *7*, 1888−1895.

(6) De Volder, M. F. L.; Tawfick, S. H.; Baughman, R. H.; Hart, A. J. Carbon Nanotubes: Present and Future Commercial Applications. *Science* **2013**, *339*, 535−539.

(7) Wong, M.; Paramsothy, M.; Xu, X. J.; Ren, Y.; Li, S.; Liao, K. Physical Interactions at Carbon Nanotube-Polymer Interface. *Polymer* **2003**, *44*, 7757−7764.

(8) Liu, Y. T.; Zhao, W.; Huang, Z. Y.; Gao, Y. F.; Xie, X. M.; Wang, X. H.; Ye, X. Y. Noncovalent Surface Modification of Carbon Nanotubes for Solubility in Organic Solvents. *Carbon* **2006**, *44*, 1613−1616.

(9) Garate, H.; De Falco, A.; Moreno, M. S.; Fascio, M. L.; Goyanes, S.; D'Accorso, N. B. Influence of Electronic Distribution of Polymers in the Spatial Conformation of Polymer Grafted Carbon Nanotube Composites. *Phys. B* **2012**, *407*, 3184−3187.

(10) Roumeli, E.; Papageorgiou, D. G.; Tsanaktsis, V.; Terzopoulou, Z.; Chrissafis, K.; Avgeropoulos, A.; Bikiaris, D. N. Amino-Functionalized Multiwalled Carbon Nanotubes Lead to Successful Ring-Opening Polymerization of Poly(ε-caprolactone): Enhanced Interfacial Bonding and Optimized Mechanical Properties. *ACS Appl. Mater. Interfaces* **2015**, *7* (21), 11683−11694.

(11) Khare, S. K.; Khabaz, F.; Khare, R. Effect of Carbon Nanotube Functionalization on Mechanical and Thermal Properties of Cross-Linked Epoxy-Carbon Nanotube Nanocomposites: Role of Strengthening the Interfacial Interactions. *ACS Appl. Mater. Interfaces* **2014**, *6*, 6098−6110.

(12) Yoonessi, M.; Lebrón-Colón, M.; Scheiman, D.; Meador, M. A. Carbon Nanotube Epoxy Nanocomposites: The Effects of Interfacial Modifications on the Dynamic Mechanical Properties of the Nanocomposites. *ACS Appl. Mater. Interfaces* **2014**, *6*, 16621−16630.

(13) Enotiadis, A.; Litina, K.; Gournis, D.; Rangou, S.; Avgeropoulos, A.; Xidas, P.; Triantafyllidis, K. Nanocomposites of Polystyrene-*b*-Poly(isoprene)-*b*-Polystyrene Triblock Copolymer with Clay-Carbon Nanotube Hybrid Nanoadditives. *J. Phys. Chem. B* **2013**, *117*, 907−915.

(14) Kang, Y.; Taton, A. Micelle-Encapsulated Carbon Nanotubes: A Route to Nanotube Composites. *J. Am. Chem. Soc.* **2003**, *125*, 5650−5651.

(15) Gegenhuber, T.; Gröschel, A. H.; Löbling, T. I.; Drechsler, M.; Ehlert, S.; Förster, S.; Schmalz, H. Noncovalent Grafting of Carbon Nanotubes with Triblock Terpolymers: Toward Patchy 1D Hybrids. *Macromolecules* **2015**, *48*, 1767−1776.

(16) Yerushalmi-Rozen, R.; Szleifer, I. Utilizing Polymers for Shaping the Interfacial Behavior of Carbon Nanotubes. *Soft Matter* **2006**, *2*, 24−28.

(17) Bates, F. S.; Hillmyer, M. A.; Lodge, T. P.; Bates, C. M.; Delaney, K. T.; Fredrickson, G. H. Multiblock Polymers: Panacea or Pandora's Box? *Science* **2012**, *336*, 434−440.

(18) Garate, H.; Morales, N. J.; Goyanes, S.; D'Accorso, N. B. In *Handbook of Epoxy Blends*; Parameswaranpillai, J., Hameed, N., Pionteck, J., Woo, E. M., Eds.; Springer International Publishing AG: Cham, Switzerland, 2015.

(19) Garate, H.; Goyanes, S.; D'Accorso, N. B. Controlling Nanodomain Morphology of Epoxy Thermosets Modified with Reactive Amine-Containing Epoxidized Poly(styrene-*b*-isoprene-*b*-styrene) Block Copolymer. *Macromolecules* **2014**, *47*, 7416−7423.

(20) Ritzenthaler, S.; Court, F.; Girard-Reydet, E.; Leibler, L.; Pascault, J. P. ABC Triblock Copolymers/Epoxy-Diamine Blends. 2. Parameters Controlling the Morphologies and Properties. *Macromolecules* **2003**, *36*, 118−126.

(21) Jia, L.; Petretic, A.; Molev, G.; Guerin, G.; Manners, I.; Winnik, M. A. Hierarchical Polymer-Carbon Nanotube Hybrid Mesostructures by Crystallization-Driven Self-Assembly. *ACS Nano* **2015**, *9*, 10673−10685.

(22) Li, Y.; Yang, D.; Adronov, A.; Gao, Y.; Luo, X.; Li, H. Covalent Functionalization of Single-Walled Carbon Nanotubes with Thermoresponsive Core Cross-Linked Polymeric Micelles. *Macromolecules* **2012**, *45*, 4698−4706.

(23) Yang, Z.; Xue, Z.; Liao, Y.; Zhou, X.; Zhou, J.; Zhu, J.; Xie, X. Hierarchical Hybrids of Carbon Nanotubes in Amphiphilic Poly(ethylene oxide)-*block*-polyaniline through a Facile Method: From Smooth to Thorny. *Langmuir* **2013**, *29*, 3757−3764.

(24) Gegenhuber, T.; Krekhova, M.; Schobel, J.; Gröschel, A. H.; Schmalz, H. "Patchy" Carbon Nanotubes as Efficient Compatibilizers for Polymer Blends. *ACS Macro Lett.* **2016**, *5*, 306−310.

(25) Esposito, H. L.; Ramos, J. A.; Mondragon, I.; Kortaberria, G. Nanostructured Thermosetting Epoxy System Modified with Poly(isoprene-*b*-methyl metacrylate) Diblock Copolymer and Polyisoprene-Grafted Carbon Nanotubes. *J. Appl. Polym. Sci.* **2013**, *129*, 1060−1067.

(26) Esposito, L. H.; Ramos, J. A.; Kortaberria, G. Dispersion of Carbon Nanotubes in Nanostructured Epoxy Systems for Coating Application. *Prog. Org. Coat.* **2014**, *77*, 1452−1458.

DOI: 10.1021/acsami.6b13212
ACS Appl. Mater. Interfaces 2017, 9, 930−943

(27) Martin-Gallego, M.; Verdejo, R.; Gestos, A.; Lopez-Manchado, M. A.; Guo, Q. Morphology and Mechanical Properties of Nanostructured Thermoset/Block Copolymer Blends with Carbon Nanoparticles. *Composites, Part A* **2015**, *71*, 136−143.
(28) Gardea, F.; Glaz, B.; Riddick, J.; Lagoudas, D. C.; Naraghi, M. Energy Dissipation Due to Interfacial Slip in Nanocomposites Reinforced with Aligned Carbon Nanotubes. *ACS Appl. Mater. Interfaces* **2015**, *7*, 9725−9735.
(29) Li, T.; Heinzer, M. J.; Francis, L. F.; Bates, F. S. Engineering Superior Toughness in Commercially Viable Block Copolymer Modified Epoxy Resin. *J. Polym. Sci., Part B: Polym. Phys.* **2016**, *54*, 189−204.
(30) Garate, H.; Fascio, M. L.; Mondragon, I.; D'Accorso, N. B.; Goyanes, S. Surfactant-Aided Dispersion of Polystyrene-Functionalized Carbon Nanotubes in a Nanostructured Poly(styrene-*b*-isoprene-*b*-styrene) Block Copolymer. *Polymer* **2011**, *52*, 2214−2220.
(31) Albuerne, J.; Boschetti-de-Fierro, A.; Abetz, C.; Fierro, D.; Abetz, V. Block Copolymer Nanocomposites Based on Multiwall Carbon Nanotubes: Effect of the Functionalization of Multiwall Carbon Nanotubes on the Morphology of the Block Copolymer. *Adv. Eng. Mater.* **2011**, *13*, 803−810.
(32) Garate, H.; Mondragon, I.; D'Accorso, N. B.; Goyanes, S. Exploring Microphase Separation Behavior of Epoxidized Poly(styrene-*b*-isoprene-*b*-styrene) Block Copolymer Inside Thin Epoxy Coatings. *Macromolecules* **2013**, *46*, 2182−2187.
(33) Garate, H.; Mondragon, I.; Goyanes, S.; D'Accorso, N. B. Controlled Epoxidation of Poly(styrene-*b*-isoprene-*b*-styrene) for the Development of Nanostructured Epoxy Thermosets. *J. Polym. Sci., Part A: Polym. Chem.* **2011**, *49*, 4505−4513.
(34) Gudzinowicz, B. J. Quantitative Determination of Ethylene Epoxide, Propylene Epoxide, and Higher Molecular Weight Epoxides Using Dodecanothiol. *Anal. Chem.* **1960**, *32*, 1520−1522.
(35) Lin, X. M.; Jaeger, H. M.; Sorensen, C. M.; Klabunde, K. J. Formation of Long-Range-Ordered Nanocrystal Superlattices on Silicon Nitride Substrates. *J. Phys. Chem. B* **2001**, *105*, 3353−3357.
(36) Ooi, S. K.; Cook, W. D.; Simon, G. P.; Such, C. H. DSC Studies of the Curing Mechanisms and Kinetics of DGEBA Using Imidazole Curing Agents. *Polymer* **2000**, *41*, 3639−3649.
(37) Guzmán, D.; Ramis, X.; Fernández-Francos, X.; Serra, A. New Catalysts for Diglycidyl Ether of Bisphenol A Curing Based on Thiol-Epoxy Click Reaction. *Eur. Polym. J.* **2014**, *59*, 377−386.
(38) Loureiro, R. M.; Amarelo, T. C.; Abuin, S. P.; Soulé, E. R.; Williams, R. J. J. Kinetics of the Epoxy-Thiol Click Reaction Initiated by a Tertiary Amine: Calorimetric Study Using Monofunctional Components. *Thermochim. Acta* **2015**, *616*, 79−86.
(39) Pittenger, B.; Erina, N.; Su, C. In *Nanomechanical Analysis of High Performance Materials, Solid Mechanics and Its Applications*; Tiwari, A., Ed.; Springer: Dordrecht, Netherlands, 2014.
(40) Hutter, J. L.; Bechhoefer, J. Calibration of Atomic-Force Microscope Tips. *Rev. Sci. Instrum.* **1993**, *64*, 1868−1873.
(41) Chyasnavichyus, M.; Young, S. L.; Geryak, R.; Tsukruk, V. V. Probing Elastic Properties of Soft Materials with AFM: Data Analysis for Different Tip Geometries. *Polymer* **2016**, *102*, 317−325.
(42) Maugis, D. *Contact, Adhesion and Rupture of Elastic Solids*; Springer-Verlag: Berlin, 2000.
(43) Butt, H.-J.; Cappella, B.; Kappl, L. Force Measurements with the Atomic Force Microscope: Technique, Interpretation and Applications. *Surf. Sci. Rep.* **2005**, *59*, 1−152.
(44) Kassman, A.; Jacobson, S.; Erickson, L.; Hedenqvist, P.; Olsson, M. A New Test Method for the Intrinsec Abrasion Resistance of Thin Coatings. *Surf. Coat. Technol.* **1991**, *50*, 75−84.
(45) Quercia, G.; Grigorescu, I.; Contreras, H.; Di Rauso, C.; Gutierrez Campos, D. Friction and Wear Behavior of Several Hard Materials. *Int. J. Refract. Hard Met.* **2001**, *19*, 359−369.
(46) Archard, J. F. Contact and Rubbing of Flat Surfaces. *J. Appl. Phys.* **1953**, *24*, 981−989.
(47) Rutherford, K.; Hutchings, I. A Micro-Abrasive Wear Test, with Particular Application to Coated Systems. *Surf. Coat. Technol.* **1996**, *79*, 231−239.
(48) Van Krevelen, D. W. *Properties of Polymers*; Elsevier Scientific Publishing Co.: Amsterdam, 1990.
(49) Peponi, L.; Tercjak, A.; Torre, L.; Kenny, J. M.; Mondragon, I. Morphological Analysis of Self-assembled SIS Block Copolymer Matrices Containing Silver Nanoparticles. *Compos. Sci. Technol.* **2008**, *68*, 1631−1636.
(50) Bilalis, P.; Katsigiannopoulos, D.; Avgeropoulos, A.; Sakellariou, G. Non-Covalent Functionalization of Carbon Nanotubes with Polymers. *RSC Adv.* **2014**, *4*, 2911−2934.
(51) Makarova, T. L.; Zakharchuk, I.; Geydt, P.; Lahderanta, E.; Komlev, A. A.; Zyrianova, A. A.; Lyubchyk, A.; Kanygin, M. A.; Sedelnikova, O. V.; Kurenya, A. G.; Bulusheva, L. G.; Okotrub, A. V. Assessing Carbon Nanotube Arrangement in Polystyrene Matrix by Magnetic Susceptibility Measurements. *Carbon* **2016**, *96*, 1077−1083.
(52) Ramasubramaniam, R.; Chen, J.; Liu, H. Homogeneous Carbon Nanotube/Polymer Composites for Electrical Applications. *Appl. Phys. Lett.* **2003**, *83*, 2928−2930.
(53) Bauhofer, W.; Kovacs, J. Z. A Review and Analysis of Electrical Percolation in Carbon Nanotube Polymer Composites. *Compos. Sci. Technol.* **2009**, *69*, 1486−1498.
(54) Hameed, N.; Guo, Q.; Xu, Z.; Hanley, T. L.; Mai, Y.-W. Reactive Block Copolymer Modified thermosets: Highly Ordered Nanostructures and Improved Properties. *Soft Matter* **2010**, *6*, 6119−6129.
(55) Peponi, L.; Valentini, L.; Torre, L.; Mondragon, I.; Kenny, J. M. Surfactant Assisted Selective Confinement of Carbon Nanotubes Functionalized with Octadecylamine in a Poly(styrene-b-isoprene-b-styrene) Block Copolymer Matrix. *Carbon* **2009**, *47*, 2474−2480.
(56) González-Domínguez, J. M.; Ansón-Casaos, A.; Díez-Pascual, A. M.; Ashrafi, B.; Naffakh, M.; Backman, D.; Stadler, H.; Johnston, A.; Gómez, M.; Martínez, M. T. Solvent-Free Preparation of High-Toughness Epoxy-SWCNT Composite Materials. *ACS Appl. Mater. Interfaces* **2011**, *3*, 1441−1450.
(57) González-Domínguez, J. M.; Martínez-Rubí, Y.; Díez-Pascual, A. M.; Ansón-Casaos, A.; Gómez-Fatou, M.; Simard, B.; Martínez, M. T. Reactive Fillers Based on SWCNTs Functionalized with Matrix-based Moieties for the Production of Epoxy Composites with Superior and Tunable Properties. *Nanotechnology* **2012**, *23*, 285702−285715.
(58) Serrano, E.; Tercjak, A.; Kortaberria, G.; Pomposo, J. A.; Mecerreyes, D.; Zafeiropoulos, N. E.; Stamm, M.; Mondragon, I. Nanostructured Thermosetting Systems by Modification with Epoxidized Styrene-Butadiene Star Block Copolymers. Effect of Epoxidation Degree. *Macromolecules* **2006**, *39*, 2254−2261.
(59) Karippal, J. J.; Narasimha Murthy, H. N.; Rai, K. S.; Krishna, M.; Sreejith, M. The Processing and Characterization of MWCNT/Epoxy and CB/Epoxy Nanocomposites Using Twin Screw Extrusion. *Polym.-Plast. Technol. Eng.* **2010**, *49*, 1207−1213.
(60) Arras, M. L.; Schillai, C.; Jandt, K. D. Enveloping Self-Assembly of Carbon Nanotubes at Copolymer Micelle Cores. *Langmuir* **2014**, *30*, 14263−14269.
(61) Hameed, N.; Salim, N. V.; Hanley, T. L.; Sona, M.; Fox, B. L.; Guo, Q. Individual Dispersion of Carbon Nanotubes in Epoxy via a Novel Dispersion-curing Approach Using Ionic Liquids. *Phys. Chem. Chem. Phys.* **2013**, *15*, 11696−11703.
(62) Pfreundschuh, M.; Martinez-Martin, D.; Mulvihill, E.; Wegmann, S.; Muller, D. J. Multiparametric High-Resolution Imaging of Native Proteins by Force-Distance Curve-Based AFM. *Nat. Protoc.* **2014**, *9*, 1113−1130.
(63) Declet-Perez, C.; Francis, L. F.; Bates, F. S. Deformation Processes in Block Copolymer Toughened Epoxies. *Macromolecules* **2015**, *48*, 3672−3684.
(64) Cui, L.-J.; Geng, H.-Z.; Wang, W.-Y.; Chen, L.-T.; Gao, J. Functionalization of Multi-Wall Carbon Nanotubes to Reduce the Coefficient of the Friction and Improve the Wear Resistance of Multi-Wall Carbon Nanotube/Epoxy Composites. *Carbon* **2013**, *54*, 277−282.
(65) Holmberg, K.; Ronkainen, H.; Matthews, A. Tribology of Thin Coatings. *Ceram. Int.* **2000**, *26*, 787−795.
(66) Lee, L. H. Fracture Energetics and Surface Energetics in Polymer Wear. *ACS Symp. Ser.* **1985**, *287*, 27−38.

DOI: 10.1021/acsami.6b13212
ACS Appl. Mater. Interfaces 2017, 9, 930−943

(67) Kim, S.; Nealey, P. F.; Bates, F. S. Decoupling Bulk Thermodynamics and Wetting Characteristics of Block Copolymer Thin Films. *ACS Macro Lett.* **2012**, *1*, 11−14.
(68) Li, T.; Heinzer, M. J.; Redline, E. M.; Zuo, F.; Bates, F. S.; Francis, L. F. Microstructure and Performance of Block Copolymer Modified Epoxy Coatings. *Prog. Org. Coat.* **2014**, *77*, 1145−1154.
(69) Hsu, S.-H.; Wu, M.-C.; Chen, S.; Chuang, C.-M.; Lin, S.-H.; Su, W.-F. Synthesis, Morphology and Physical Properties of Multi-Walled Carbon Nanotube/Biphenyl Liquid Crystalline Epoxy Composites. *Carbon* **2012**, *50*, 896−905.
(70) Zhang, L. C.; Zarudi, I.; Xiao, K. Q. Novel Behavior of Friction and Wear of Epoxy Composites Reinforced by Carbon Nanotubes. *Wear* **2006**, *261*, 806−811.

DOI: 10.1021/acsami.6b13212
ACS Appl. Mater. Interfaces 2017, 9, 930−943